

LA-UR -78-876

MASTER

CONF - 780324 - - 3

TITLE: DESIGN ENGINEERING OF LARGE HIGH-PRESSURE
GAS LASER AMPLIFIERS

AUTHOR(S): W. T. Leland

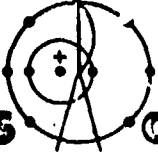
SUBMITTED TO: Invited Paper
SPIE Technical Symposium East '78
Washington, DC
March 28-31, 1978

NOTICE

This report was prepared as an account of work sponsored by the United States Government. Neither the United States nor the United States Department of Energy, nor any of their employees, nor any of their contractors, subcontractors, or their employees, makes any warranty, express or implied, or assumes any legal liability or responsibility for the accuracy, completeness or usefulness of any information, apparatus, product or process disclosed, or represents that its use would not infringe privately owned rights.

By acceptance of this article for publication, the publisher recognizes the Government's (license) rights in any copyright and the Government and its authorized representatives have unrestricted right to reproduce in whole or in part said article under any copyright secured by the publisher.

The Los Alamos Scientific Laboratory requests that the publisher identify this article as work performed under the auspices of the USERDA.



Los Alamos
scientific laboratory
of the University of California
LOS ALAMOS, NEW MEXICO 87545

An Affirmative Action/Equal Opportunity Employer

Form No. 830
St. No. 2629
1/75

UNITED STATES
ENERGY RESEARCH AND
DEVELOPMENT ADMINISTRATION
CONTRACT W-7405-ENG. 36

22/83

DESIGN ENGINEERING OF LARGE HIGH-PRESSURE GAS LASER AMPLIFIERS

W. T. Leland
 University of California
 Los Alamos Scientific Laboratory
 Los Alamos, NM 87545

Abstract

The creation of a population inversion in large-volume high-pressure gas via an electrical discharge poses numerous engineering problems, not only concerning details of various components, but also in overall system performance or optimization. The Laser Division at Los Alamos has developed a base of engineering data and computational techniques which addresses the engineering design problems for our short-pulse, large, high-pressure CO₂ amplifiers. The various aspects of the problem considered individually and in total are:

1. Selection of gas mixture for specific application;
2. Physical specifications (size, pressure, voltage, current, etc.) of discharge to achieve desired energy output. This involves the use of computer codes to account for gas kinetics relevant to the production of a population inversion and energy-extraction codes;
3. Specification of energy supply and delivery system to provide power to the discharge. This involves computer codes to predict discharge current and voltage waveforms, taking account of various circuit elements (capacitors, inductances, and transmission lines) as well as the nonlinear character of the discharge;
4. Nonuniformities in discharge and population inversion resulting from magnetic field effects, finite geometry, etc. This involves computer codes which consider electron trajectories in the high-pressure gas in the presence of electric and magnetic fields as well as the nonlinear characteristic of the discharge.

The calculational techniques have been used to design a prototype amplifier for the Los Alamos 100-kw Antares system. The prototype was built and the design calculations confirmed by measurements.

Introduction

Because of its simplicity and high efficiency, the CO₂ gas laser has undergone extensive study and development. Several review articles¹⁻⁴ survey the knowledge that has been amassed on CO₂ lasers. At Los Alamos, this information, coupled with specialized studies² and development work, has been used to design large short-pulse CO₂ amplifiers for use in laser-fusion research. Described below are a few considerations and procedures used in the field of CO₂ laser engineering.

General Considerations

The requirements of large energies (tens of kilojoules) in short-pulse durations (a nanosecond or less) create most of the unique design problems encountered. With the large energies it is desirable to use high flux densities to minimize size and cost. Consideration of damage thresholds in optical components⁵ has led to the selection of 2 J/cm² as a practical design level for transmitting elements such as windows. Reflecting elements which handle 4 J/cm² can be obtained. The population inversion in CO₂ lasers occurs between vibrational levels in the electronic ground state. Superimposed on the vibrational levels are the rotational levels and, on a nanosecond time scale, the energy exchange rate between rotational levels⁶ can substantially affect the amount of energy that can be extracted, as well as the temporal shape of the amplified pulse. In addition to gain saturation effects, energy extraction and pulse shape in the nanosecond regime also require due consideration of bandwidth and coherent phenomena. For efficient performance, high gas pressure is favored since the rotational energy transfer time varies inversely with pressure, and line broadening (or bandwidth) is directly proportional to pressure. Simultaneous extraction of energy on several lines (rotational levels) is also very desirable, but must be weighed against the increased system complexities it entails. Preliminary design and tradeoff studies are usually made with approximate energy extraction calculations, as will be described later. Final design performance is checked with computer calculations, which

include all known relevant phenomena such as rotational relaxation and coherent effects.

High gas pressure is also desirable in order to obtain a high density of energy storage and consequently smaller size amplifiers. Energy storage density for a given gas mixture and temperature is proportional to the product of pressure and small-signal gain. Since pumping (inversion creation) efficiency and parasitic oscillation development place practical limits on small-signal gain, high-energy storage density generally dictates high-pressure operation.

Apart from the usual practical difficulties of operating at high pressures (construction of pressure vessels, higher discharge voltages, etc.) an upper limit to the pressure results from gas optical breakdown whose threshold varies inversely with pressure.

Choice of Amplifier Type

Two types of high-pressure CO₂ amplifiers are currently in general use: those employing self-sustained electrical discharges and those which use an external source of high-energy electrons to provide the gas ionization for maintaining the electrical discharge (e-beam sustained). At their present state of development, each type has special virtues and limitations. Self-sustained discharge amplifiers are limited in size to a gap-width-times-pressure product (PD) of about 20 cm atmospheres, operate at greater than optimal electric-field-to-number-density ratio (E/N), and generally utilize gas mixtures not optimal for nanosecond-pulse amplifiers. They are, however, capable of producing a very uniform amplifier medium and are generally considered to be simpler than e-beam-sustained amplifiers, which require the addition of a high-voltage electron gun. E-beam-sustained amplifiers can be made to operate with much larger PD values (units now in use operate with PD values over 75). They can be operated with optimal gas mixtures and E/N values. Uniformity in the amplifier medium is difficult to achieve in the very large amplifiers. Any nonuniformity in spatial distribution of ionization from the external electron beam results in nonuniformities in the discharge. Magnetic fields from the discharge current can severely affect the trajectories of the electrons from the external gun and thus cause nonuniform ionization. At Los Alamos, the large power amplifiers are chosen to be e-beam units because of the size limitations on self-sustained types. Pre-amplifier stages typically are self-sustained discharge amplifiers.

Choice of Gas Mixture

Gas mixtures chosen for nanosecond-pulse amplifiers differ from those used in most applications. Nitrogen is used in laser gas mixtures because it readily exchanges its vibrational energy with the upper laser level in CO₂ molecules and in effect provides a very selective channel for funneling energy from the electric discharge into the desired state of the CO₂ molecule. The CO₂ upper state level population essentially comes into equilibrium with the nitrogen levels during the pumping time (a few microseconds). During the nanosecond energy extraction time, however, no significant energy transfer from the nitrogen occurs and the energy stored in the nitrogen molecules is wasted. For this reason, the optimal mixtures for nanosecond-pulse amplifiers use less nitrogen. The best mixtures balance the benefits from selective nitrogen excitation with losses due to energy left in the nitrogen. Helium is used in most gas mixtures because of its beneficial action in relaxing the lower state population density. Because it has no low-lying states, it also permits the desired average electron energy to be attained for a lower E/N ratio in the discharge. Again, because the relaxation process is inconsequential during a nanosecond, helium is not beneficial in short-pulse amplifiers except where operation at lower E/N ratios is of great importance. In very large-volume amplifiers, the use of helium could, for economic reasons, require a helium recovery system.

Table I provides data on three different gas mixtures. The first two are used in Los Alamos nanosecond-pulse amplifiers, while the third is more typical of mixtures used in other applications. All values refer to a gas pressure of 1800 torr, a temperature of 300 K, a discharge energy of 150 J/l at optimum E/N, and a current density of 15 A/cm².

TABLE I
COMPARISON OF CO₂ LASER GAS MIXTURES

	Mixture Proportions He:N ₂ :CO ₂		
	0:1:4	12:1:4	3:2:1
g(%/cm)	3.75	3.50	2.43
Inversion Energy (J/l)	21.1	15.2	10.9
Line Width ⁹ (GH, FWHM)	13.0	10.0	10.0
Rotational Relaxation ⁶ Time Constant (PS)	43	69	61
Optimum Electric Field (kV/cm)	18	10.5	15
Electron Drift Velocity (10 ⁶ cm/s)	8.9	5.6	5.7
Recombination Coefficient (10 ⁻⁷ cm ⁻³ s ⁻¹)	6	9	--

Values for rotational relaxation and line width are based on data as referenced. Small-signal gain and energy storage for the specified input are calculated using Los Alamos computer codes for handling CO₂ laser kinetics in an electrical discharge.

The helium-free mixture is substantially more efficient for a nanosecond pulse. It is also superior in terms of desired values of rotational relaxation time and line width. The higher E/N ratio for the helium-free mixture presents mixed values to the electrical engineer. While the higher voltages required may cause problems, the implied higher impedance of the discharge is a definite plus.

Energy Extraction Calculations

In the tradeoff studies leading to selection of a final design to meet a given set of requirements, the considerations regarding gas pressure and composition discussed above remain as parameters. Energy extraction calculations must be made for each set of parameters. To facilitate preliminary tradeoff studies, the energy extraction calculation is treated on the basis of an equivalent two-level Frantz-Nodvik¹⁰ formulation:

$$E_{out} = E_s \ln \left[1 + e^{gL} (e^{E_{in}/E_s} - 1) \right], \quad (1)$$

where E_{in} and E_{out} are the input and output energies per unit area. gL is the product of small-signal gain and amplifier length. E_s is an "effective" saturation energy which depends on gas mixture, pulse duration, gas pressure, and number of lines used. For cases of interest at Los Alamos, an approximation by G. Schappert is used:¹¹

$$E_s \approx \frac{\Delta E \Delta N K M}{2g} \left[1 - \left(\frac{1-KM}{KM} \right) \left(\exp(-\tau_p KM / \tau_r) - 1 \right) \right], \quad (2)$$

where M is the number of lines used for energy extraction, K is the average fraction of molecules in the upper level which are in each of the M lines. τ_p and τ_r are the pulse length and rotational relaxation time, respectively. $\Delta E \Delta N K M$ is to be interpreted as the total inversion energy in the M lines.

Values for E_s are shown in Fig. 1 for a one-nanosecond pulse in a helium-free mixture.

Magnetic Field Effects and Calculation of Discharge Current and Potential Distribution

Available window sizes presently limit the area of a single amplifier to about 30 x 30 cm. With these large electrode spacings, close attention must be paid to the effects of magnetic fields on discharge uniformity. In the absence of external fields, high-energy electrons from the electron gun follow a random zigzag path as they proceed through the high-pressure gas. If the magnetic field becomes too large, it can overcome the randomization effects of gas

scattering and cause nonuniformity in path distributions. Assessment of the severity of the problem can be made by comparing the electron scattering length with its radius of curvature in the magnetic field. Figure 2 depicts such a comparison with a gas pressure of three atmospheres in a helium-free mixture.¹² Scattering length (defined as mean path length required to produce an angular deviation of one radian via multiple scattering) is plotted as a function of electron energy. The radius of curvature is also plotted for various magnetic fields. The preferred region of operation is above and to the left of the scattering length curve. Note that operation in this region can always be achieved if the electron energy is sufficiently low. On the other hand, the electron energy must be great enough to traverse the aperture. The distribution of electron trajectories for each design is checked with a Monte Carlo calculation¹³ using the appropriate geometry and including applied electric and magnetic fields. The result is an ionization rate distribution such as shown in Fig. 3. This particular distribution is for a prototype amplifier built to verify the design of the 100 kJ (Antares) amplifiers. The prototype amplifier medium is 130 cm long and has a cross-sectional area of 25 x 30 cm. It is designed to operate with 1800 torr of helium-free mixture and with a discharge voltage of 500 kV. With the calculated ionization distribution, a second calculation is performed which yields the distribution of current and electric field in the discharge. The calculation solves the equations

$$\nabla \cdot \vec{j} = 0 \quad (3)$$

$$\vec{j} = \frac{S(\vec{r})}{\gamma} e v_d \quad (4)$$

subject to boundary conditions (electrodes at fixed potentials). \vec{j} is the current density and e the electronic charge. $S(\vec{r})$ is the ionization rate at point \vec{r} as given by the Monte Carlo calculations described above.

γ and v_d are the recombination coefficient and drift velocity, both of which depend on the local E/N ratio. Figure 4 shows the dependence of γ and v_d on E/N for a helium-free mixture. v_d is based on calculations that solve the Boltzmann equation using energy-dependent cross sections for the interaction of electrons with molecules.¹⁴ γ is derived from experimental work performed at Los Alamos.

An example of calculated current and voltage distribution is shown in Fig. 5. It is for the prototype and uses the ionization rate distribution of Fig. 3. In Fig. 6 the calculated current density is compared with actual measurements.

Small-Signal Gain Magnitude and Distribution

The attained value of small-signal gain or population inversion depends on the amount and duration of voltage and current delivered to the discharge. The actual current and voltage depend in turn on the power supply design, the power delivery arrangement, and the impedance of the discharge. Approximate values of current and voltage needed are selected with the aid of curves such as those in Fig. 7 where calculated small-signal gain is shown for a series of different current densities at a fixed value of electric field. However, with an actual amplifier/power-supply combination, neither the current nor voltage is likely to be constant. The final check on whether a given design will produce the required performance is made by calculating the waveform of current and voltage expected with the chosen power-supply system driving the nonlinear load presented by the discharge. These current and voltage waveforms are then used along with the CO_2 gas kinetics to calculate the actual performance.

Continuing with the prototype example considered earlier, gain calculations are compared with measured values in Figs. 8 and 9, which show the small-signal gain distribution and time history of small-signal gain, respectively.

Summary

The above paragraphs give a brief description of various problems facing the engineer in the selection of a "best" design for a CO_2 discharge to meet a given set of requirements. Many interacting parameters are at his disposal, but few display true optimal values within the range permitted by practical constraints. The performance of a given design is amenable to calculation, albeit quite complex. Simplified approximate calculations and design aids are

available for most tradeoff studies. A good preliminary design can then be checked by more elaborate calculations. The calculations have been applied to a large prototype amplifier and found to give good agreement with observed performance.

References

1. O. R. Wood, II, "High-Pressure Pulsed Molecular Lasers," Proc. of the IEEE, 62, 355-397 (1974).
2. T. F. Stratton, "CO₂ Short-Pulse Laser Technology," in High Power Gas Lasers 1975, E. R. Pike, Ed. (The Institute of Physics, Bristol, 1976), pp. 284-311.
3. P. K. Cheo, "CO₂ Lasers," in Lasers, Vol. 3, A. K. Levine and R. J. DeMaria, Eds. (Marcel Dekker, Inc., New York, 1971), Chap. 3, pp. 111f.
4. R. L. Taylor and S. Bitterman, "Survey of Vibrational Relaxation Data for Processes Important in the CO₂-N₂ Laser System," Rev. Mod. Phys., 41, 26-46 (1969).
5. J. J. Hayden and I. Liberman, "Measurements at 10.6 μ m of Damage Threshold in Germanium, Copper, Sodium Chloride, and Other Optical Materials at Levels up to 10¹⁰ W/cm²," in Laser Induced Damage in Optical Materials, 1976 NBS Special Publication 462 (U.S. Dept. of Commerce 1976)
6. R. Jacobs, K. J. Pettipiece, S. J. Thomas, "Rotational Relaxation Rate Constants for CO₂," Appl. Phys. Lett., 24, 375-377 (1974).
7. B. J. Feldman, "Multiline Short-Pulse Amplifications and Compression in High Gain CO₂ Laser Amplifiers," Optics Comm., 14, 13-16 (1975).
8. P. J. Berger and D. C. Smith, "Gas Breakdown in the Laser as the Limitation of Pulsed High-Pressure CO₂ Lasers," Appl. Phys. Lett., 21 167-170 (1972).
9. R. L. Abrams, "Broadening Coefficients for the P(20) CO₂ Laser Transition," Appl. Phys. Lett., 25, 609-611 (1974).
10. L. M. Frantz and J. S. Nodvik, "Theory of Pulse Propagation in a Laser Amplifier," J. Appl. Phys., 34, 2346-2349 (1963).
11. G. T. Schappert, Los Alamos Scientific Laboratory, Unpublished Data, May 1975.
12. J. C. Comly, Jr., Los Alamos Scientific Laboratory, Unpublished Data, 1977.
13. D. B. Henderson, "Electron Transport in Gas Discharge Lasers," J. Appl. Phys., 44, 5513-5515 (1973).
14. J. J. Lowke, A. V. Phelps, and B. W. Irwin, "Predicted Electron Transport Coefficients and Operating Characteristics of CO₂:N₂:He Laser Mixtures," J. Appl. Phys., 44, 4664-4671 (1973).

FIGURE CAPTIONS

Fig. 1. Effective saturation parameter for a 1-ns pulse in 1:4::N₂:CO₂ mixture calculated using Eq. (2).

Fig. 2. Electron scattering length (L) and radius of curvature (r₀) for various magnetic fields vs electron energy in 2280 torr of 1:4::N₂:CO₂ mixture.

Fig. 3. Predicted ionization density in the prototype discharge region. Contours are shown where the relative ionization produced by the primary beam drops to 0.9, 0.7, 0.4, and 0.1 of its maximum value (indicated by the +). The primary beam energy was 440 keV, and a self-consistent magnetic field was imposed.

Fig. 4. Drift velocity (v_d) and recombination coefficient (γ) for 1:4::N₂:CO₂ mixture.

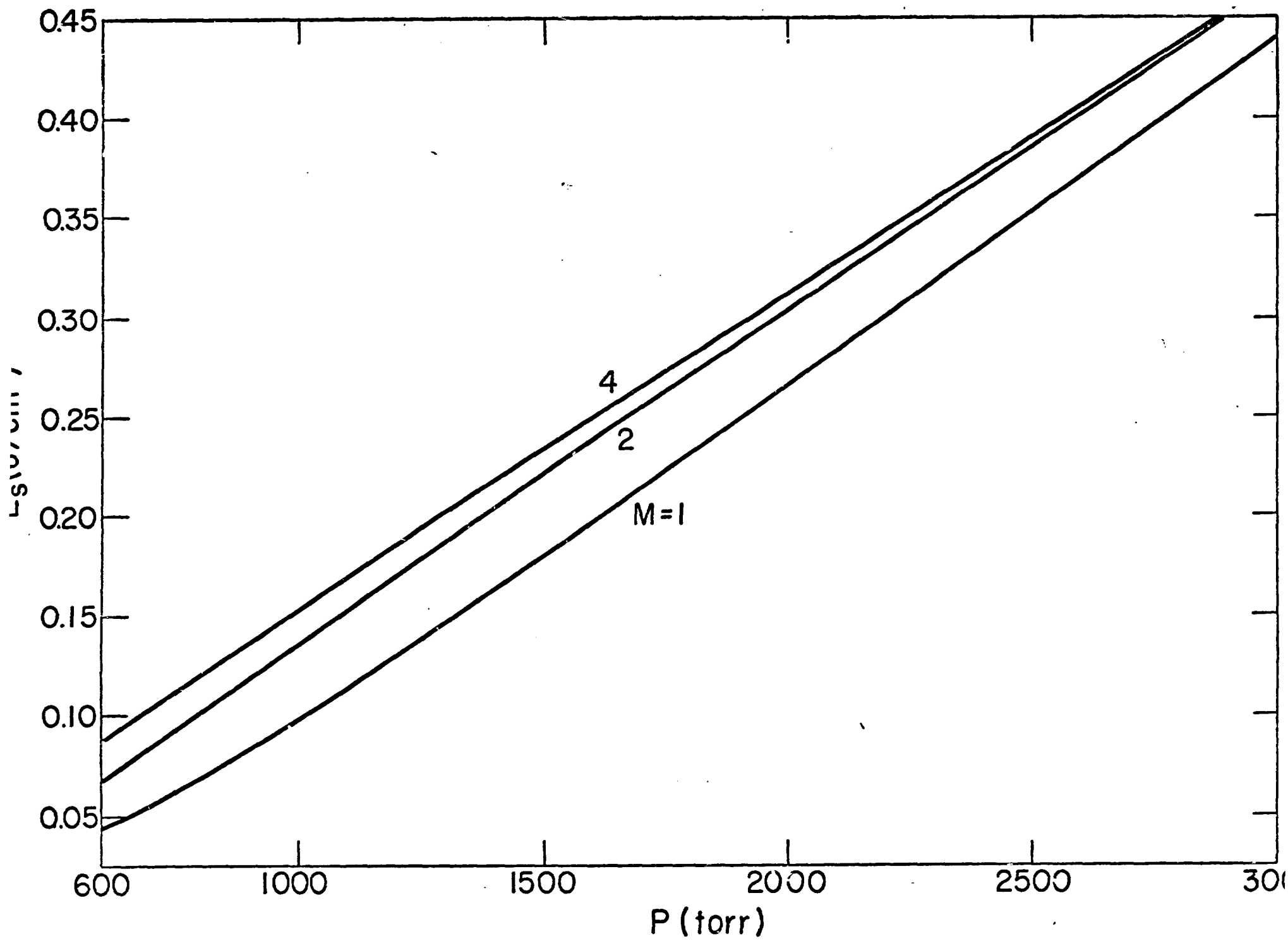
Fig. 5. Lines of equal current and potential in prototype.

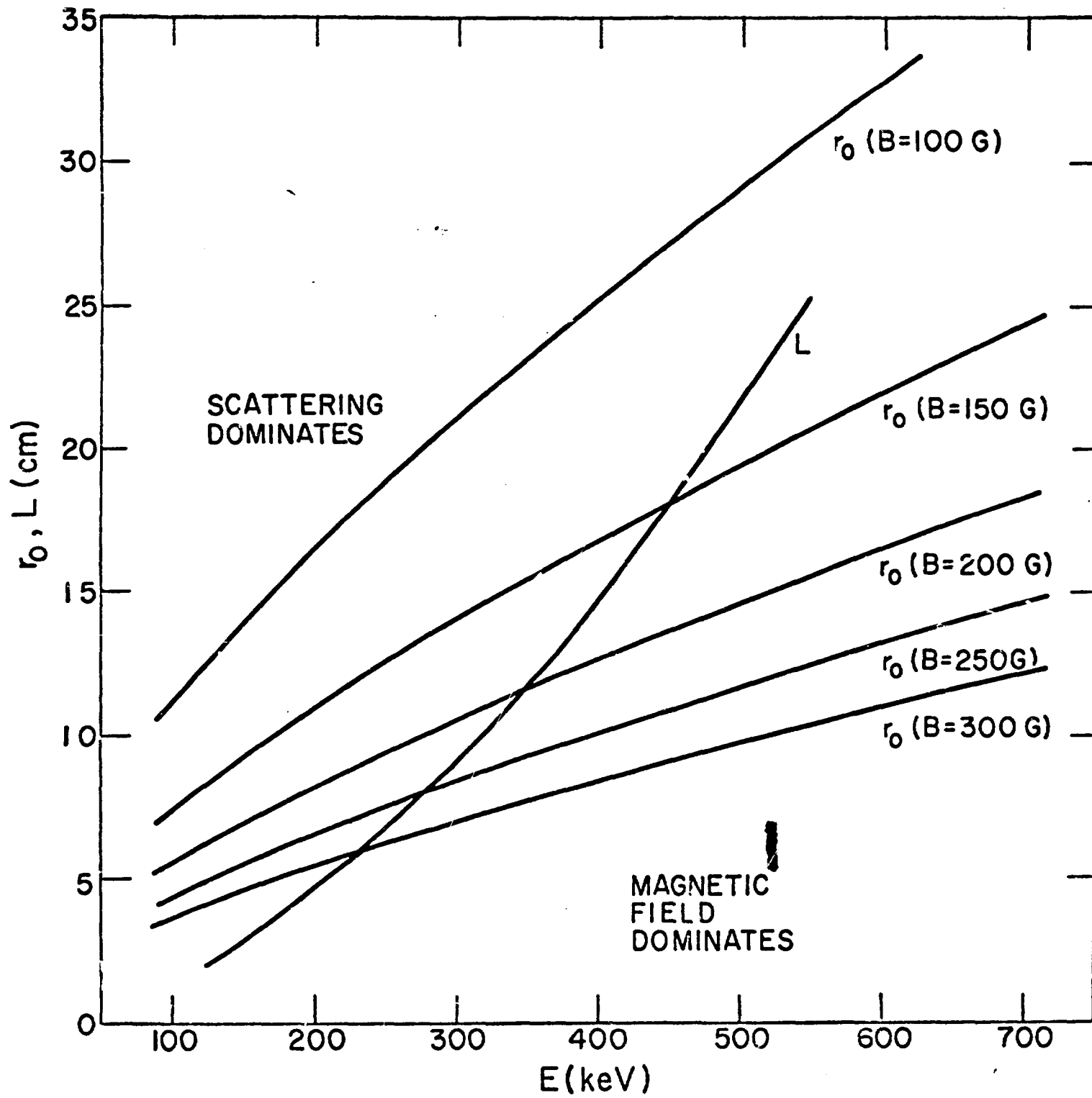
Fig. 6. Comparison of calculated and experimental discharge current distribution.

Fig. 7. Calculated small-signal gain for various current densities and a fixed field.

Fig. 8. Calculated (●) and measured \bar{g} at the center of the discharge.

Fig. 9. Time-history comparison of experimental and calculated small-signal gain.





F-5

6.01E
Fig. 3

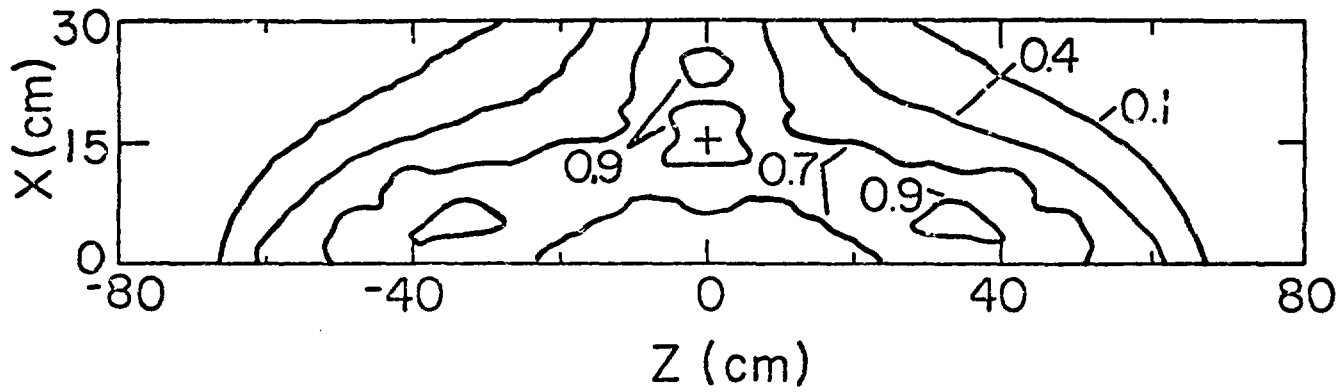
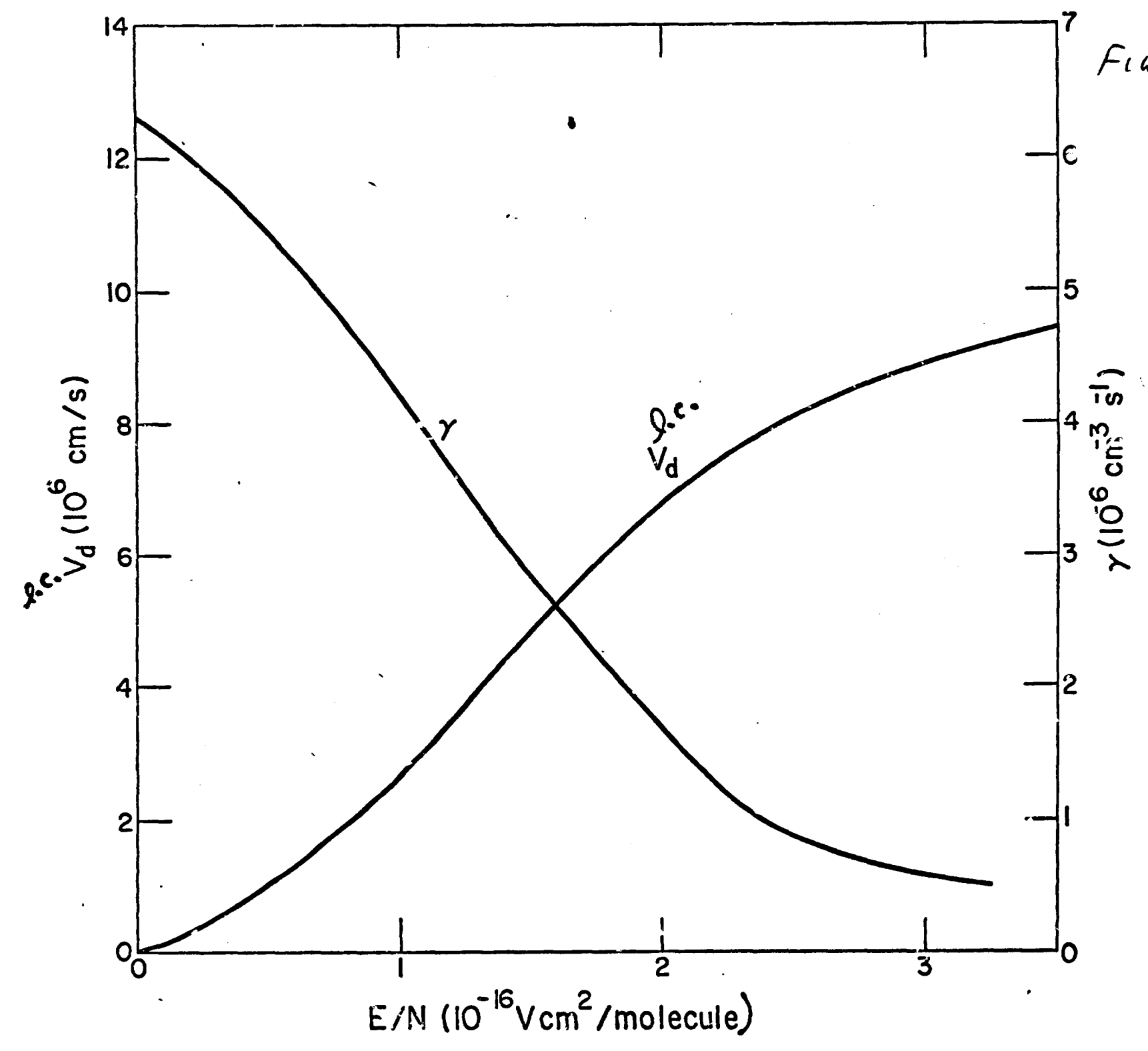
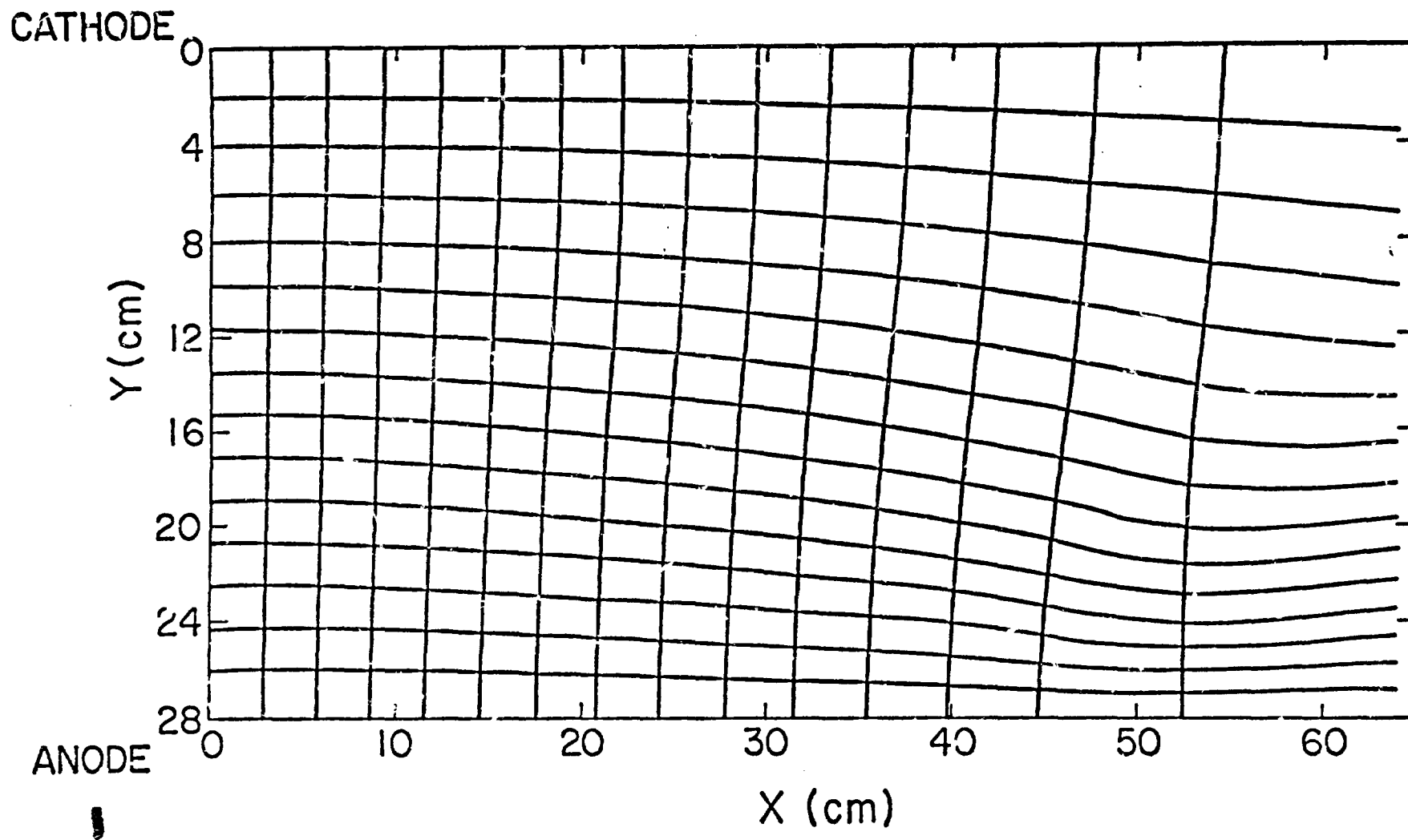
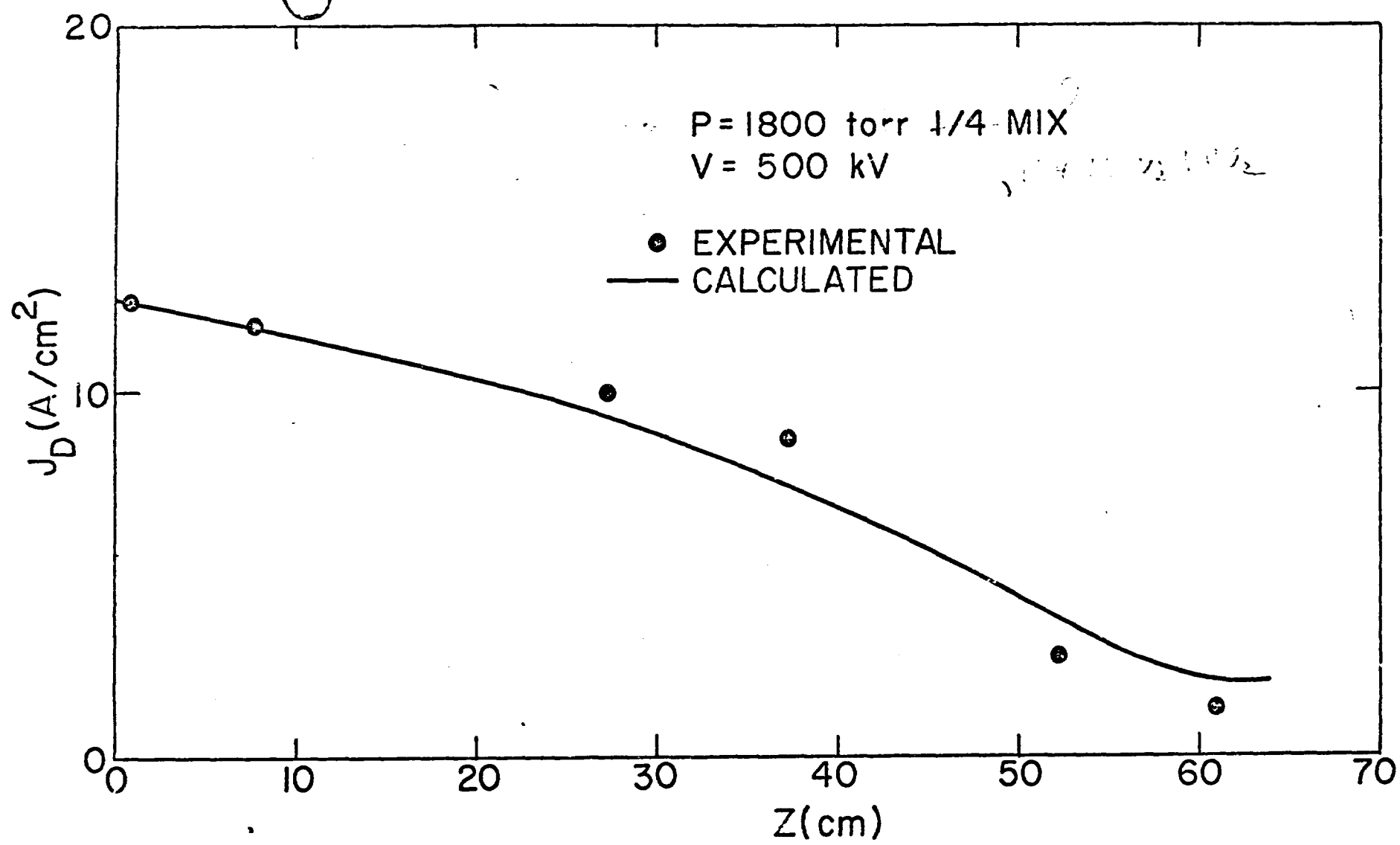


FIGURE 7







COMPARISON OF CALCULATED AND EXPERIMENTAL DISCHARGE CURRENT DISTRIBUTION



77-11832
FIGURE 7

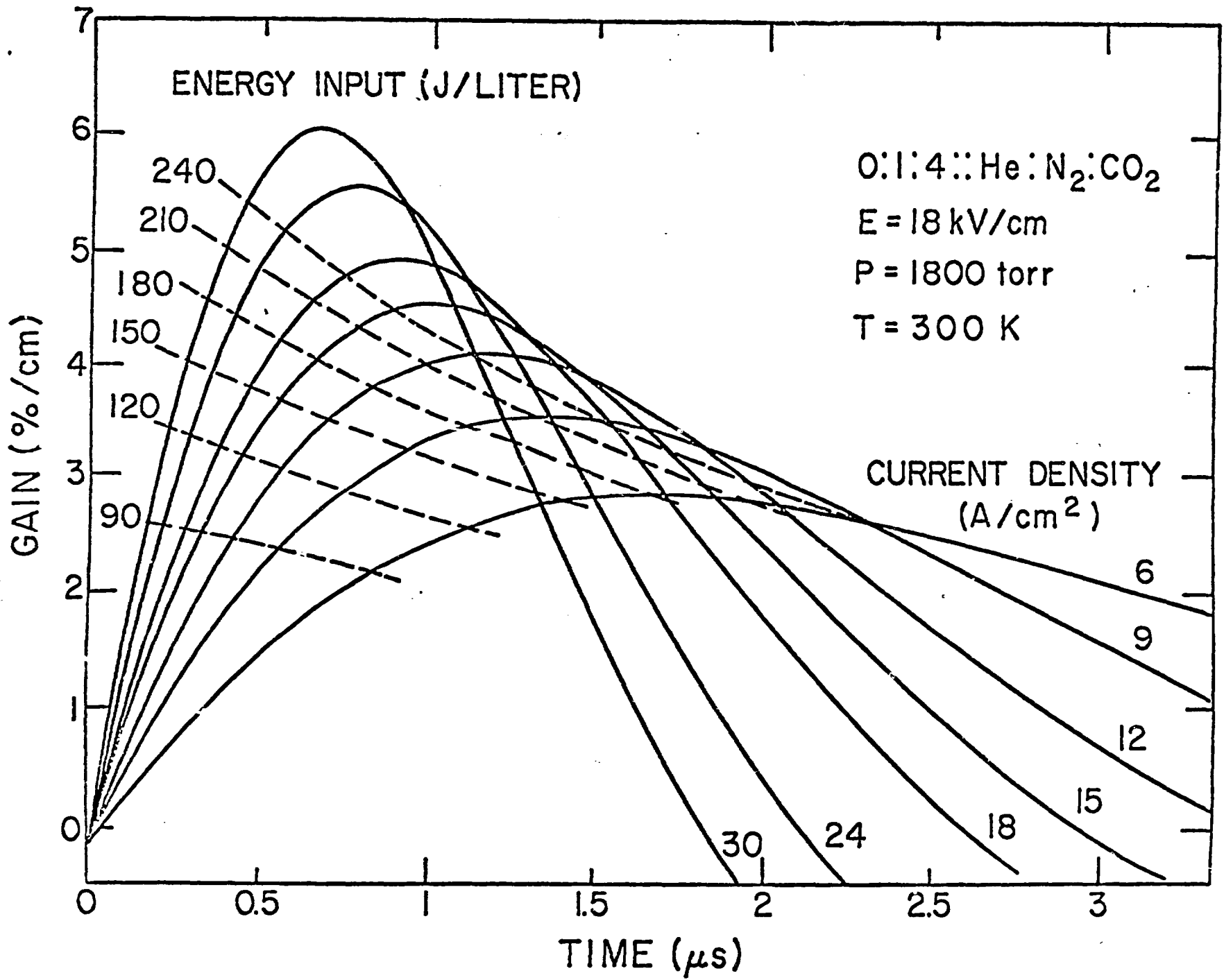


FIGURE 8

